

Cite this: *J. Mater. Chem. C*, 2021,
9, 5689

The liquid crystal Click procedure for oligothiophene-tethered phthalocyanines – self-assembly, alignment and photocurrent†‡

Moritz Dechant,^a Matthias Lehmann,^{id}*^{ab} Genya Uzurano,^c Akihiko Fujii^{id}^c and Masanori Ozaki^{id}^c

A series of star-shaped liquid crystals (LCs) with a phthalocyanine donor core, oligothiophene antennae and fullerene acceptors have been successfully prepared. This hierarchical self-assembly results in a nanosegregated helical donor–acceptor–antennae LC-system promoted by the recently discovered Click procedure. This model system reveals all photophysical prerequisites for energy conversion, charge generation and transport. Uniform amorphous thin films of 150 nm could be produced by bar-coating. Annealing did not only induce the formation of columns *via* the Click procedure but also partially homeotropically aligned the non-clearing sample in a sandwich geometry (ITO and Ag/MoO₃). This has been confirmed by microscopic studies and the measurement of photocurrent, which increased by a factor of 300 after the annealing step.

Received 12th February 2021,
Accepted 15th March 2021

DOI: 10.1039/d1tc00710f

rsc.li/materials-c

1. Introduction

Recently, phthalocyanines or porphyrins attached to conjugated oligomers and polymers have attracted much attention owing to their promising properties for organic electronic applications.^{1,2} Dyads with fullerenes have also been prepared for photovoltaic applications.^{3–10} Long-lived charge carrier separation was reported⁶ and the dyads were mixed with conjugated polymers realizing absorption over the full visible spectral range, which added a light-harvesting effect.^{11,12} Many liquid-crystalline dyads have been synthesized in order to combine high order and the propensity for alignment – both properties are needed to improve the efficiency of organic electronic devices.^{13–23} Although large ambipolar and balanced charge carrier mobilities have been found for a columnar double cable structure, no photovoltaic applications from such dyads are reported.¹⁶ All these features have recently been combined in shape-persistent star mesogens. One parent star compound provides intrinsic free

space between its arms and one is a shape-amphiphile, in which the flat star mesogen is connected to four spherical fullerenes *via* flexible spacers.^{24–26} The latter compound is sterically overcrowded existing only as an amorphous material. However, a 1:1 mixture of the two stars generates triple-nanosegregated helical columnar liquid-crystalline phases, in which the fullerenes occupy the free space of the parent stars. This process is called the Click procedure, which is based on the shape-amphiphilicity and driven by the nanosegregation tendency of the fullerenes and the filling of the void space. This phase realizes almost an ideal donor–acceptor double cable structure of phthalocyanines locked in the center of the columns surrounded by a quadruple helical fullerene structure. The conjugated oligomers in between act as additional light harvesters (antennae) transferring the absorbed energy to the phthalocyanine center.

The molecules were provided with peripheral oligo (ethyleneoxy) chains, which should lower the transition temperature to the isotropic phase (clearing temperature). This is needed for the conventional alignment of the material, in which cooling from the isotropic phase between two substrates results in standing columns like molecular cables connecting the electrodes (homeotropic alignment of a columnar phase). Additionally, these polar flexible chains should increase the dielectric constant of the material to promote charge separation and prevent recombination. Unfortunately, the clearing temperature remained above 300 °C and all the attempts to align the sample failed.²⁷ Here, we present phthalocyanine star mesogens equipped with oligothiophene arms as excellent organic semiconductors²⁸ and to prevent photoreactions known for the frequently applied

^a Institute of Organic Chemistry, University of Würzburg, Am Hubland,
97074 Würzburg, Germany. E-mail: Matthias.Lehmann@uni-wuerzburg.de

^b Center for Nanosystems Chemistry, University of Würzburg, Theodor-Boveri-Weg,
97074 Würzburg, Germany

^c Graduate School of Engineering, Osaka University, 2-1 Yamada-oka,
Suita, Osaka 565-0871, Japan

† In memory of Professor Siegfried Hünig.

‡ Electronic supplementary information (ESI) available: Synthetic procedures, molecule spectroscopy data, GPC elugrams, density measurements, X-ray data, modelling, alignment, photoelectron yield spectroscopy data, and *I*–*V* measurements. See DOI: 10.1039/d1tc00710f

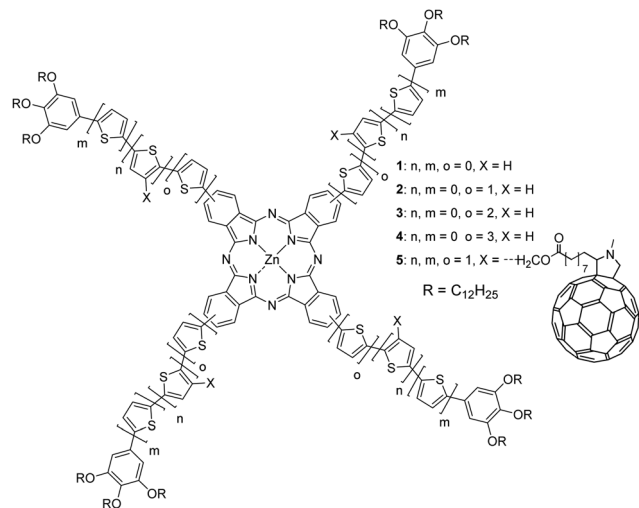


Fig. 1 Target molecules 1–5.

oligo(phenylenevinylene) scaffolds (Fig. 1).²⁹ The oligothiophene arms were capped with phenyl rings decorated with aliphatic chains, replacing the oligo(ethyleneoxy) chains of the previous system. Since earlier results demonstrated that oligo(ethyleneoxy) chains have little impact in bringing down the clearing temperatures to practical values, this structural modification enabled us to reduce the complexity of the synthesis. The free space providing LC star mesogens 1–4 and the sterically overcrowded non-LC fullerene derivative 5 have been successfully prepared. Their thermotropic properties have been studied and the self-assembly using the Click procedure for the 1 : 1 mixture of compounds 4 and 5 has been demonstrated. This procedure resembles supramolecular recognition procedures, especially the CPI effect proposed by Boden and Bushby,³⁰ which has been previously summarized and discussed.²⁵ The new 1 : 1 mixture has been comprehensively studied according to its photophysical properties. The LC could be partially aligned by annealing in a sandwich geometry, which resulted in a significantly increased photocurrent.

2. Synthesis

All target molecules 1–5 (Fig. 1) were synthesized by following a convergent route, in which the corresponding dicyano-functionalized arms without fullerenes were condensed in a tetracyclomerization to afford the phthalocyanines (Scheme 1). Only in the subsequent step, an esterification with a fullerene derivative results in the sterically overcrowded compound 5. The arms for compounds 1–4 were built by a series of Suzuki–Miyaura and bromination reactions beginning with precursor 6. The 3,4-dicyano derivatives 11, 10a–c were tetracyclomerized in the last step to give the star-mesogens 1–4 in moderate yields between 15% and 37%.

For the synthesis of the sterically overcrowded derivative 5, a hydroxymethyl function had to be introduced. Starting with the commercially available boronic acid 12, esterification, reduction and a protection step with dihydropyran yielded the building block 15 with the protected hydroxymethyl anchor (Scheme 1).

This group could be attached to the dicyano derivative 8a to yield 16 and subsequently 17 by bromination. The following Suzuki–Miyaura cross coupling with 9b furnished the arm 18. Tetracyclomerization of 18 and acidic cleavage of the THP-protective groups resulted in an insoluble material owing to side reactions. Therefore, the THP-groups have been cleaved prior to the tetracyclomerisation to yield 19 (91%), which gave subsequently the fullerene derivative 5 in 24% yield in the last two steps – tetracyclomerisation and fourfold esterification.²⁴

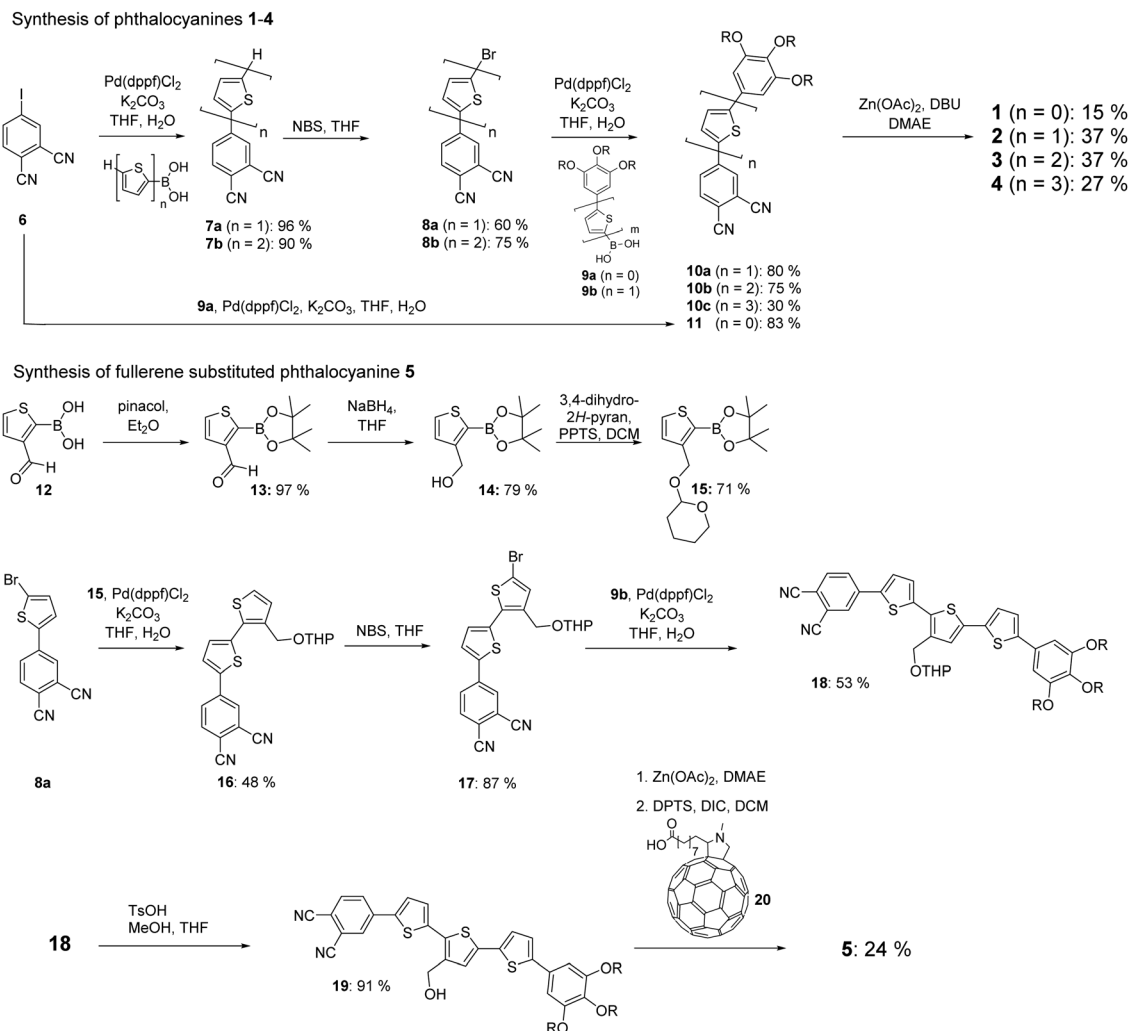
All compounds were characterized by standard analytical methods (NMR, mass spectrometry, elemental analysis; see the ESI†). The purity of target structures is demonstrated by a single peak in the elugram after recycling GPC (see Fig. S10, ESI†). The characterization by ¹H and ¹³C NMR spectroscopy is challenging since they exhibit generally broad signals^{31,32} owing to aggregation and the presence of four regioisomers – the (2,9,16,24)-, (2,9,17,24)-, (2,10,16,24)- and (2,9,16,23)-isomers, which are typically obtained in a statistical ratio of 4:2:1:1 during the synthesis.³¹ The aggregation increased with the size of the stars. Thus resolved ¹H NMR spectra were obtained for compounds 1–3 in either CD₂Cl₂ or THF-*d*₈ or by the addition of some pyridine-*d*₅ which revealed phthalocyanine protons typically in the range of 7.7–9.5 ppm, thienyl protons between 7.2 and 8.0 ppm and peripheral aromatic protons from 6.6 ppm to 7.3 ppm (Fig. S1–S3, ESI†).³⁰ The ¹H NMR spectrum of the largest compound 4 revealed distinct protons only at a high temperature of 378 K in C₂D₂Cl₄ (Fig. S4, ESI†). The ¹³C NMR spectra revealed exclusively broad signals.¹⁴ The analysis has been especially challenging for compound 5, which exhibited poorly resolved spectra even at higher temperatures (398 K, see Fig. S5–S7, ESI†). However, compounds 4 and 5 were unambiguously characterized by HRMS mass spectrometry, for which the signal of the product could clearly be observed and the experimental and simulated isotopic patterns were in excellent agreement (Fig. 2).

Furthermore, the IR spectrum of compound 5 confirms the absence of free OH groups and the strong peak at 1735 cm^{−1} corroborates that the ester group formed successfully during the fourfold Steglich esterification (see Fig. S11, ESI†). The presence of the ester and the fullerenes is further verified by ¹³C NMR spectroscopy, which shows a broad signal at 172 ppm and rather prominent, unresolved signals for the fullerene carbons between 140 and 155 ppm.

3. Thermotropic properties

The thermotropic properties of all compounds were studied by polarized optical microscopy (POM), differential scanning calorimetry (DSC) and X-ray scattering (XRS).

Star mesogen 1 clears into the isotropic phase over a broad temperature range beginning at 249 °C. A typical texture for a columnar phase was obtained by slow cooling of the sample from the isotropic phase (Fig. 3A). In contrast, compounds 2–4 do not clear (see Fig. S9B–D, ESI†), but decompose at temperatures above 350 °C. This prevented the formation of characteristic textures. The DSC results confirm the absence of phase transitions



Scheme 1 Synthesis of the target compounds **1–5** ($R = C_{12}H_{25}$).

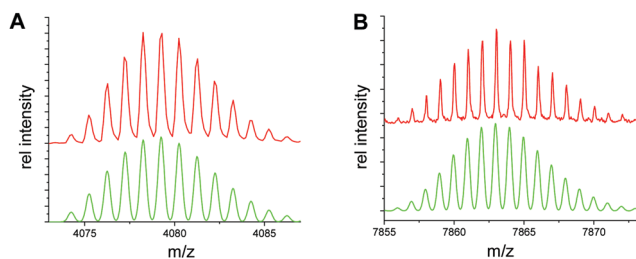


Fig. 2 Comparison of the experimental (red) and simulated (green) HRMS-MALDI spectra of compounds **4** (A) and **5** (B). For full range MALDI spectra see the ESI.†

from ambient temperature up to 300 °C for **2–4**. In the case of these compounds, the liquid-crystallinity was confirmed by shearing (**2**, **3** at 150 °C, **4** at 180 °C) resulting in planar aligned mesophases (Fig. 3B, E and H). In contrast, the sterically overcrowded fullerene derivative exhibits only an amorphous solid without any birefringence. The mixtures of compounds **4** and **5** also do not clear and reveal only one phase over the whole temperature range. The 1:1 mixture can be sheared above

220 °C, furnishing a beautiful, planar aligned film (Fig. 3K). The improved alignment of the mixture compared with the neat compounds **4** and **5** hints at a special self-assembly, which will be shown to originate from the Click procedure. Insertion of the λ -compensator reveals that the largest refractive indices of the samples add to the slow axis of the compensator when the shearing direction is orthogonal to the latter. This confirms that the phthalocyanines are essentially oriented perpendicular to the columnar structures (Fig. 3C, D, F, G, I, J, L and M).

3.1 X-Ray scattering and modelling

Detailed structural information of compounds **1–4** has been derived for aligned fibers by temperature-dependent wide-angle X-ray scattering (WAXS). Fig. 4 highlights all WAXS patterns. They reveal signals typical for columnar liquid crystals – a series of equatorial reflections reminiscent of the 2D lattice of columns, a halo attributed to the average distance of the hydrocarbons, namely the liquid-like chains, and signals corresponding to 3.4–3.7 Å indicating π - π stacking of the phthalocyanine discs. Only compound **1** forms a soft crystal below 180 °C with a rather large c -parameter pointing to a

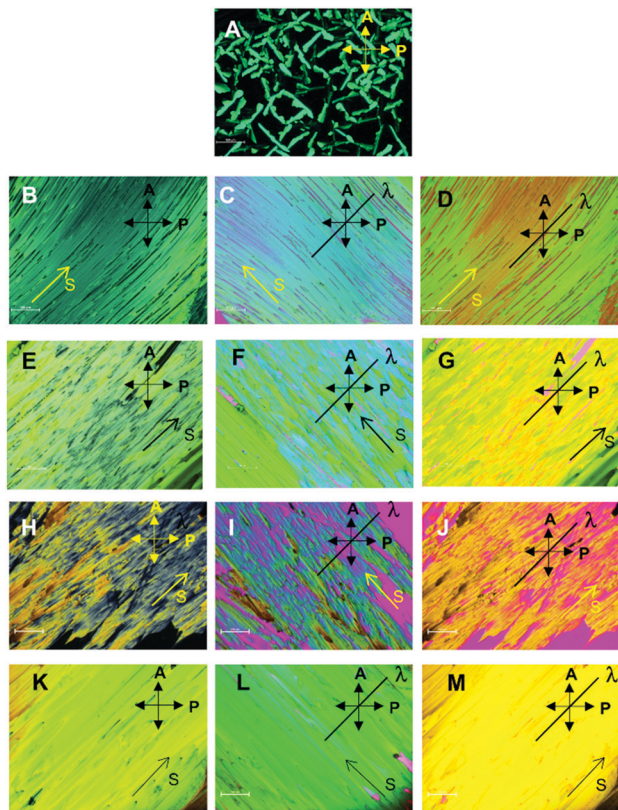


Fig. 3 Texture of **1** after cooling from the isotropic phase at 130 °C (A), POM texture of shear aligned compounds **2** (B–D), **3** (E–G), **4** (H–J) and the 1:1 mixture of **4** and **5** (K–M). (S: shearing direction, P: polarizer, A: analyser, λ : direction of the slow axis of the compensator plate.) The λ -compensator confirms the optical negative nature of columnar phases (C, D, F–J, L and M).

helical arrangement (Fig. S20, ESI \ddagger). At higher temperatures, the large number of meridional small angle signals disappears and remained absent even upon cooling to 25 °C. Only the annealing at 160 °C resulted in the reformation of the soft crystal. The liquid crystal phase does not exhibit any sign of 3D correlations. The equatorial signals might be indexed to a hexagonal phase; however, the splitted π - π signals at all temperatures indicate the tilt of the discs between 27 and 35°, and thus the phase is better described as a centered rectangular phase which is related to the hexagonal phase with $b_{\text{rec}} = a_{\text{hex}}$ and $a_{\text{rec}} = 2a_{\text{hex}} \sin 60^\circ$. Moreover, a slight deviation from this exact relationship would explain the rather broad signals and result in better fitting. Compound **1** is a compact disc with a large number of chains. The difference in packing distance of the chains and aromatic building block results in the optimization of the stacking distance by tilting and in the formation of the rectangular phase, especially when the mobile flexible chains occupy a growing volume with increasing temperature. This can also be observed for the next larger molecule **2**, which possesses a hexagonal columnar phase at ambient temperature, but the increasing splitting of the π - π signals above 150 °C indicates the formation of a centered rectangular phase. For both compounds, the repeating unit

contains one molecule per column, confirmed by density measurements (see the ESI \ddagger), and thus these compounds are rather classical discotics. Similar X-ray patterns but without any splitting of the π - π -signals up to the highest accessible temperature (250 °C) are obtained for compounds **3** and **4**. Interestingly, compound **4** improves its alignment after the extrusion procedure only in the more fluid phase above 220 °C.

The core diameters of the molecules obtained from molecular models increase by approximately 7 Å with the addition of a thiophene repeating unit. The columnar diameters for molecules **1**–**3** also increase by 6–7 Å, while there is evidently a larger jump in the columnar diameter by 9 Å for compound **4** (see Table S2, ESI \ddagger). In a columnar slice of only 3.4 Å thickness for compound **4**, density considerations predict two molecules that obviously cannot stack on top of each other, and thus it is reasonable that they arrange side by side in a dimer, in order to compensate for the rather large intrinsic free space between the arms. This also explains the rather large increase in the columnar diameter.²⁵ A possible model is a helical organization of dimers, which was previously discussed for other derivatives based on diffuse meridional scattering intensities, indicating periodicity along the columns.²⁴ For mesogen **4**, the diffuse intensity superimposed on the 21 reflections is discerned as well. This points to helical stacks of a short correlation length. The double helical stacking further explains the less efficient π -stacking visualized by the low intensity of the wide angle reflection.

The obvious dimer formation of compound **4**, and thus the compensation of the intrinsic free space, makes it a suitable system to test a different compensation mode like the recently discovered Click mechanism with a sterically overcrowded fullerene star.²⁴ The XRS results for different mixtures of **4** and **5** are highlighted in comparison with the neat samples **4** and **5** in Fig. 4G–M. Note that the sterically overcrowded compound **5** exhibits only an X-ray pattern of an amorphous phase. All mixtures were extruded at 180 °C and the virgin fibers reveal only broad reflections with some preorganization and almost no π - π -stacking signals. Only heating to the more fluid phase at 220 °C furnished patterns pointing to a higher organization, indicating the Click procedure. The most pronounced π - π -stacking is observed for the 1:1 mixture. A slight access of the sterically overcrowded component **5** results directly in a much lower level of organization. Yet, also a lower content of star **5** affords a reduced degree of order of the self-assembly, demonstrated by the weak π - π -stacking signal. The equatorial reflections of the 1:1 mixture correspond to a hexagonal lattice with an a -parameter of 54.7 Å at 25 °C. This enormous decrease of the columnar diameter compared with the dimer phase of compound **4** by more than 6 Å combined with the strong π - π -stacking signal is clear evidence for the loss of the lateral packed homodimer phase in favor of coplanar stacked heterodimers of **4** and **5**. This demonstrates the operation of the Click procedure,^{24–26} in which fullerenes fill the intrinsic free space between arms and the phthalocyanines are locked in the middle of the column. The π - π -stacking distance at 25 °C amounts to 3.3 Å, and thus one mesogen **4** and one

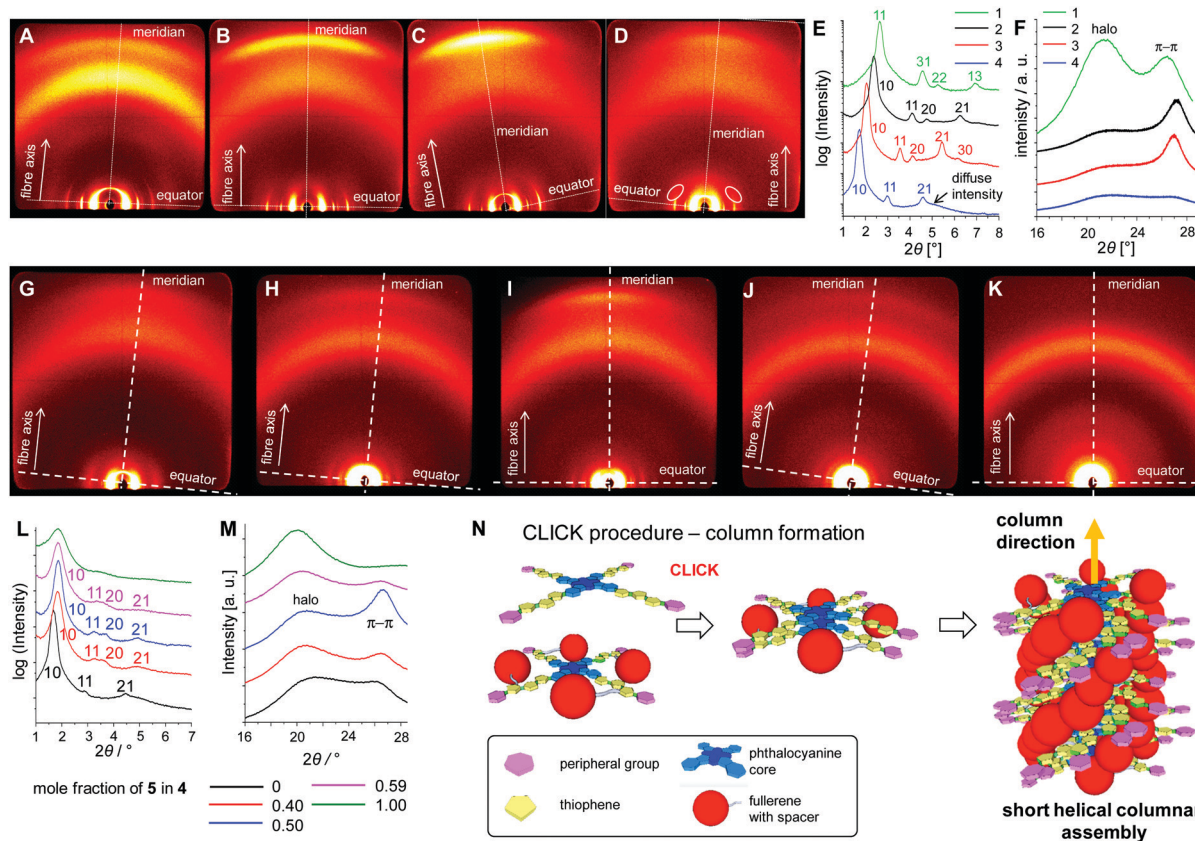


Fig. 4 2D WAXS patterns of the centred Col_h -phase after cooling of **1** (A, 25 °C) and the Col_h -phases of **2** (B, 150 °C), **3** (C, 250 °C), and **4** (D, 250 °C), the diffuse meridional intensities are highlighted with white ellipses. (E) Integrated intensity along the equator of the patterns with indexation confirming the different columnar structures. (F) Integrated intensity along the meridian showing the halo (average chain distance) and the variation of the intensity for the signal attributed to the π - π -interaction at room temperature. WAXS patterns (25 °C) of **4** (G) and the mixtures of **4** and **5** with increasing mole fraction of compound **5**: (H) 0.40, (I) 0.50, (J) 0.59, and (K) 1. (L) Integrated intensity along the equator of the patterns with indexation confirming the Col_h structure for mixtures with increasing mole fraction of compound **5**. (M) Comparison of the WAXS region (meridian) for mixtures with increasing mole fraction of compound **5**. (N) Model of the Click procedure and the formation of short helical columns of the 1 : 1 mixture of **4** and **5**.

mesogen **5** assemble in a stack of 6.6 Å along the columnar axis. This leads to a reasonable density of $1.142 \pm 0.040 \text{ g cm}^{-3}$, which is in acceptable agreement with the experimentally observed density of the material ($1.186 \pm 0.006 \text{ g cm}^{-3}$). The difference in the height of the heterodimer between **4** and **5** ($h = 6.7 \text{ Å}$) and the diameter of a fullerene (10.3 Å) reveal that in a model of this columnar phase the fullerenes need to be interdigitated along the column, which is best realized with a helical displacement of the fullerenes highlighted previously.^{24,33,34} The correlation length of the π - π -stacking along the c -axis is 26.9 Å, and thus only eight molecules are correlated in a stack. This explains naturally why the X-ray intensity attributed to the periodical, helical packing could not be observed, since only very short helical stacks are formed.

Fig. 4N highlights schematically the Click process and the formation of the helical column with a short correlation length. A geometry optimized model of such helical fragments with seven heterodimers is visualized in Fig. S19 (ESI \ddagger). The model (Fig. 4N and Fig. S19, ESI \ddagger) reveals a triple nanosegregated donor-acceptor quadruple helix. This comprises the nanosegregation of the aromatic part in a zinc phthalocyanine center, which possesses a shell of helically segregated

fullerenes and oligothiophenes. The residual volume of the unit cell is filled by the additionally nanosegregated aliphatic chains. The model further indicates that the fullerenes of different columns approach each other and the formation of interwoven fullerene networks is feasible (Fig. S19, ESI \ddagger).³⁴

4. Photophysical properties

Fig. 5 highlights the photophysical behavior of the series of compounds **1**-**5** in THF and thin films. Fig. 5A shows the UV-Vis spectra in solution, which appear as superpositions of the different building blocks – oligothiophene bands with maxima at 356 nm (**2**), 379 nm (**3**), 418 nm (**4**) and 405 nm (**5**); phthalocyanine Soret bands with a maximum at 362 nm (**1**) and superimposed maxima for **2**-**5**; Q bands with maxima at 688 nm (**1**), 710 nm (**2**), 715 nm (**3**), 717 nm (**4**) and 725 nm (**5**) and in the case of molecule **5** the additional fullerene absorption with maxima at 253 nm and 323 nm. The progression of the oligothiophene absorption maxima with increasing arm length is comparable to that of the neat oligothiophenes containing three to five aromatic building blocks³⁵ and superimposes with

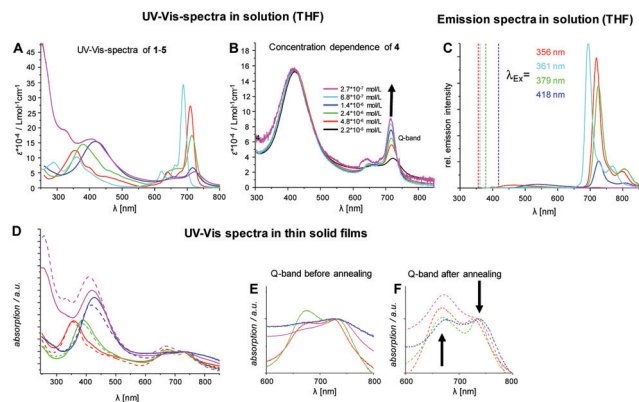


Fig. 5 UV-Vis spectra of **1** (cyan blue), **2** (red), **3** (green), **4** (blue) and **5** (purple) in THF (A). Concentration-dependent UV/Vis studies of **4** in THF (B). (C) Concentration corrected emission spectra of **1** (cyan blue, $c = 1.2 \times 10^{-7} \text{ mol L}^{-1}$), **2** (red, $c = 2.4 \times 10^{-7} \text{ mol L}^{-1}$), **3** (green, $c = 3.2 \times 10^{-7} \text{ mol L}^{-1}$), **4** (blue, $c = 3.6 \times 10^{-7} \text{ mol L}^{-1}$) and **5** (purple, $c = 2.6 \times 10^{-7} \text{ mol L}^{-1}$) in THF. Dotted lines indicate excitation wavelengths (λ_{ex}). (D) Solid state UV-Vis spectra of **2** (red), **3** (green), **4** (blue) and the mixture of **4** and **5** (magenta) before (solid lines) and after annealing (dashed lines). (E) Magnification of the Q-band before annealing. (F) Magnification of the Q-band after annealing.

the Soret band of the phthalocyanine core. Interestingly, for compound **5**, this oligothiophene band shifts hypsochromically by 13 nm compared with **4** owing to the functionalization of the scaffold to attach the fullerene. With increasing length of the conjugated oligomer, the Q-band of the ZnPc-stars, which corresponds to the π - π^* transition, moves slightly bathochromically. This clearly indicates that the conjugated arm and the core are interacting with each other. Even a minor change in the substitution pattern of **5** results in a bathochromic shift of 8 nm compared with **4**. In addition, the increasing arm length seems to influence dramatically the intensity of the maximum of the Q-band which decreases from **1** to **4**. The integral of the band between 600 and 850 nm remains almost constant for compounds **1**–**3**, indicating that the transition dipole moment does not change significantly. However, for compound **4**, the integral decreases to 60% compared with compounds **1**–**3** revealing a considerable change in the transition dipole. This can be attributed to the aggregation of **4** even at concentrations as low as $4.9 \times 10^{-6} \text{ mol L}^{-1}$. Fig. 5B demonstrates that the intensity of the Q-band increases when the concentration decreases and this is limited only by the increasing noise at a concentration of $2.7 \times 10^{-7} \text{ mol L}^{-1}$. The absorption maximum of **4** shifts hypsochromically to almost 715 nm, which equals the absorption maximum of compound **3**, indicating that this conjugated scaffold has already achieved the effective conjugation length.³⁶ Fig. 5D–F show the normalized absorption spectra of **2**–**4** and the 1:1 mixture in their thin films. The continuous lines correspond to spectra recorded before and the dotted lines correlate with spectra recorded after annealing for five minutes at 220 °C. The typical broadening of solid state spectra can be discerned. The Q-band exhibits now the low bathochromically shifted maximum for all materials pointing to aggregation, expected in the thin solid film. Except for compound **3**, all

materials possess absorption maxima at approximately 736 nm. Annealing leads in general to more defined narrow Q-bands and to an intensity increase for the hypsochromically shifted maximum at 650 nm for compound **2** and the mixture of **4** and **5**, while for compounds **3** and **4** both absorption bands at 650 nm and 736 nm are almost identical in peak height. At room temperature, the XRS results confirm for both materials **2** and the 1:1 mixture of **4** and **5** that the mesogens are coplanarily stacked, and thus the pronounced hypsochromic intensity might indicate preferred H-aggregates.³⁷ For compound **4** a double helical arrangement has been proposed by XRS with a lower organization degree of the zinc phthalocyanines. The deviation of the absorption spectrum of the annealed film of **4** compared with compound **2** reflects the difference in the molecular self-assembly. The analogous thin film spectrum of **3** points to a similar arrangement compared with material **4**. The most pronounced annealing effect for the 1:1 mixture of **4** and **5** can be attributed to the locking procedure in the middle of the column and is another experimental result pointing to the favorable aggregation by the Click process.²⁴

Fig. 5C highlights the emission spectra of compounds **1**–**5** recorded at similar concentrations and obtained by excitation in the absorption maximum of the conjugated oligothiophene. Although the conjugated arms are highly emissive (see Fig. S12, ESI†), their fluorescence is almost completely quenched by the ZnPc moiety pointing to efficient energy transfer. In contrast to the previously described oligo(phenylenevinylene) derivatives for which the Q-band emission of the ZnPcs increases in intensity when extending the arm size,²⁴ the oligothiophene stars **1**–**4** exhibit an opposite behavior. This can be in part explained by the reduced emission of the arm derivatives with an increase in size. The principle reason for the largest breakdown in Q-band fluorescence of compound **4** is, however, the formation of H-type aggregates even at concentrations as low as $2 \times 10^{-7} \text{ mol L}^{-1}$ (see Fig. 5B). Such aggregates are non-emissive.^{38,39} For the fullerene derivative **5**, the emission of the ZnPc-core is also completely quenched, which demonstrates the efficient energy transfer cascade from the conjugated oligomers to the phthalocyanine cores to the fullerene. Usually an electron transfer results between the latter, separating positive and negative charges, which was previously confirmed for a similar mesogen by femto-second spectroscopy.^{24,40–42} Therefore, the present system is an attractive material for OPV applications.

5. Electronic properties

The HOMO levels of **4**, **5** and the 1:1 mixture (before and after annealing to 220 °C for five minutes) were studied by photoelectron yield spectroscopy. HOMO–LUMO gaps were determined by absorption spectroscopy (see Table S4 and Fig. S27, ESI†). Metal phthalocyanine HOMO and LUMO energies may vary between $-(4.4\text{--}5.0) \text{ eV}$ and $-(3.1\text{--}4.4) \text{ eV}$ depending on substitution patterns and metals.^{43–45} The determined energy of 5.2 eV for ZnPc **4** is slightly above these

HOMO values and fits perfectly the ITO work function, which is 5.2 eV.⁴⁶ On the other hand, the LUMO level of **5** is identical to the value for the fullerene derivative PCBM (−3.8 eV).⁴⁷ This indicates that the energy levels would fit well for a possible application in photovoltaic cells. The most important additional precondition for engineering an acceptable LC device is the correct alignment of the columnar complex structure. For the use of the present columnar liquid crystal as photovoltaics or photodetectors, a homeotropic alignment is mandatory, in which the columns stand orthogonal between the two electrodes and connect them like molecular cables. Unfortunately, this cannot be conventionally achieved by simple cooling from the isotropic liquid, owing to the extremely high clearing point of the material. Recently, E. Grelet *et al.* found that discotics can be oriented also by annealing in the columnar liquid crystal when sandwiched between a glass substrate and a vacuum deposited metal film (Ag).²⁷ The speed of the homeotropic alignment depended strongly on the thickness of the spin-coated material. This process is only geared by the surface tension and was successfully applied in several studies.^{27,48,49}

In the present case, a 1:1 mixture of **4** and **5** has been deposited on an ITO substrate by bar-coating as a 150 nm thick, uniform film, which is non-birefringent between crossed polarizers (Fig. 6A). In contrast to conventional discotics for which bar-coating produces planar aligned columnar LC samples,⁵⁰ in the present

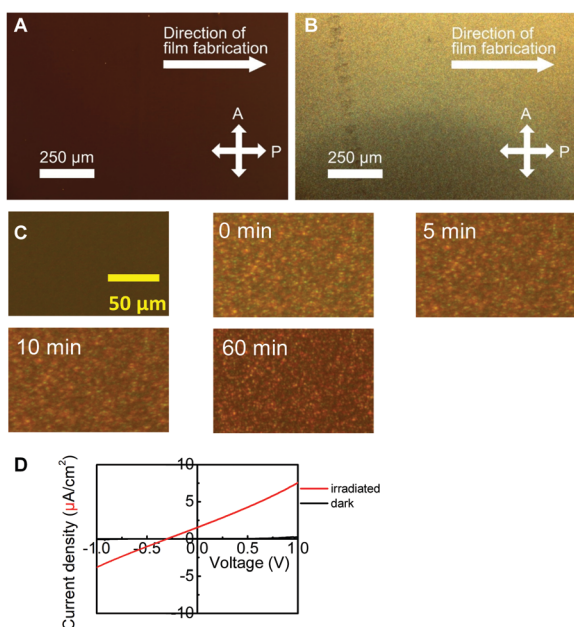


Fig. 6 Bar-coated film of the 1:1 mixture of **4** and **5** with a thickness of 150 nm. Uniform film at room temperature (A) and after 5 minutes of pre-annealing at 280 °C (B). (C) Annealing study: sandwiched bar-coated film and post-annealed film at 280 °C after 0, 5, 10 and 60 minutes. Decreasing birefringence point to slow homeotropic alignment. (D) *I*–*V* measurements with (red line) and without (black line) illumination of a sandwiched film treated with 5 minutes pre-annealing at 280 °C and 24 h post-annealing at 200 °C. The photocurrent increases by a factor of 300 after the annealing procedures.

system only amorphous films are generated. In order to improve the alignment of the films, they have been annealed either before vacuum deposition of a thin MoO₃/Ag electrode (pre-annealing) or after deposition of the electrode (post-annealing). A series of annealing procedures have been performed on different cells, followed by POM studies and the measurement of the current density profile, to qualitatively prove the correct homeotropic alignment. Pre- or post-annealing processes at temperatures ≤ 220 °C changed neither the texture nor the current density profile, indicating that the films remained in their amorphous state. Pre- or post-annealing the samples at 280 °C for 5 minutes initiated important changes. The texture became birefringent, however, without preferred orientation. Dark spots indicate that some homeotropically aligned domains are present. Nevertheless, the current density profile remained at low values for dark current and the current upon AM1.5G illumination. This changed significantly when the samples were post-annealed at 200 °C for 24 hours. As a result, the dark currents became low but the currents at illumination increased by a factor of up to 300 (Fig. 6D), although the texture did not change significantly. Textural changes have been observed, when the samples were annealed for a longer period of time at 280 °C (Fig. 6C). The images became slowly less birefringent pointing to homeotropic alignment. However, the cells prepared by post-annealing at 280 °C for 30 minutes showed high leak currents, which indicates that the cell structure or the material has been damaged.

Fig. 7 highlights a schematic model of the processes explaining these experimental observations. Bar-coating of the mixture in chlorobenzene at 60 °C produces a uniform but amorphous thin film. The Click procedure proceeds only at high temperatures, and thus no columnar aggregates are present at that step (Fig. 7, left). Cautious annealing to up to 220 °C to prevent decomposition resulted neither in any birefringence nor in changes of the very low current densities. Only at 280 °C the molecules in the thin film became mobile enough for the formation of columnar aggregates *via* the Click procedure. Subsequent self-assembly of the columns in small μm size domains (Fig. 7, right) affords a grainy birefringent texture. The post-annealing process did improve the contact to the electrodes and resulted in low dark currents and the 300 times higher current density upon illumination. We assume that this is a consequence of the low number of dark domains, which are homeotropically or almost

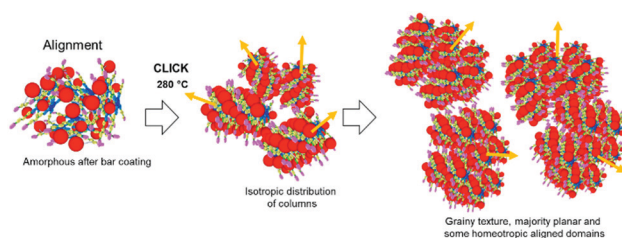


Fig. 7 Self-assembly processes observed after bar coating, pre- and post-annealing.

homeotropically aligned, while the majority of the domains are highly birefringent and do not possess the desired orientation. Nevertheless, the photocurrent increases by a factor of 300 and this was reproducibly measured with different cells. The present photocurrent is rather low compared to what is needed for real photovoltaic devices, but this is a consequence of the very limited homeotropic alignment. Nevertheless, these results are highly encouraging since they demonstrate the crucial role of the morphology and alignment of the materials. They indicate that improved properties can be expected for a material, for which the Click process and the alignment procedure start at lower temperatures and, consequently, the thermal procedure does not damage the material or the cell. Based on these findings, which reveal the promising potential of the tailor-made donor–acceptor materials, further work is currently in progress to bring down the clearing temperatures and viscosities in order to establish the optimal alignment.

6. Conclusion

In conclusion, we have synthesized successfully new shape-persistent star-mesogens with oligothiophene arms and zinc phthalocyanine cores. With increasing arm length, the intrinsic free space between the arms increases. While the first members of the series form conventional hexagonal and rectangular columnar liquid-crystalline phases, the star mesogen with three thiophene repeating units clearly packs in a double helical structure with a short correlation length, to compensate for the large void between the arms. A different compensation pathway could be uncovered by mixing the sterically overcrowded and non-mesogenic compound **5** in a ratio of 1 : 1 with the largest star **4**. In this mixture, the fullerenes fill the space between the arms and lock the zinc phthalocyanines to the center of the column. The strong segregation tendency of the fullerenes leads to short helical interdigitated fullerene strands along the column. As a result, the mesogenic core is triple nano-segregated – the zinc phthalocyanine in the center, which is helically surrounded by a nanosegregated shell of fullerenes and oligothiophenes. This is a result of the previously described Click procedure, which is working also for the present type of stars. The absorption spectroscopy supports the different packing modes in the liquid crystal systems. Photophysical studies reveal further that energy transfer as in an antenna system and aggregate formation even at very low concentrations dominate the fluorescence quenching. The most efficient quenching is observed for the fullerene containing star in which the energy cascade transfers the energy to the fullerene.

HOMO–LUMO levels have been determined to be promising for application. An alignment study clearly shows that uniform 150 nm thick films can be produced by bar coating. At 25 °C, before the Click procedure, these films are amorphous. The sandwiched film with a Ag/MoO₃ top electrode could be partially aligned using an annealing protocol, which initiated the Click process in the material to form the birefringent columnar liquid crystal. Despite the low fraction of correctly

oriented soft matter the photocurrent increases by a factor of 300. This implies the tremendous significance of the correct alignment of donor–acceptor materials for future applications. Consequently, the present outstanding nanostructured material will be extremely promising for organic photovoltaics or photo-detectors, if the alignment procedures can be optimized. These investigations are currently in progress.

6.1 XRS experiments

The temperature dependent WAXS investigations were performed on a Bruker NANOSTAR (Detector Vantec 2000, Incoatec Microfocus copper anode X-ray tube). The fibers were produced by extrusion from the liquid crystal state using a home-made miniextruder. The aligned fibers were transferred to Mark capillaries, which were sealed and glued into the metal sample holder, with the fiber direction parallel to the tilt direction of the detector (tilted by 14°). The XRS heating system was calibrated by liquid crystal standard compounds. The XRS data were evaluated using the program Datasqueeze with silver behenate as a calibration standard.⁵¹ The correlation lengths were estimated using the Scherrer formula.⁵²

6.2 Photoelectron spectroscopy

The photoelectron spectra were measured by using photoelectron yield spectroscopy (Sumitomo Heavy Industries, PYS-202-H) to determine the HOMO level. The D2 lamp light passing through a monochromator as a UV light source, the intensity of which was calibrated using a Si photo-diode, was irradiated onto the sample surface under a vacuum of 10^{−3} Pa, and the generated photo-electrons collected by the ring electrode were measured using a sub-femtoamp remote source meter (Keithley, 6430).

6.3 Bar-coating and cell production

The cleaned indium-tin-oxide (ITO)-coated glass substrates were placed on a hotplate and the substrate temperature was set at 60 °C, and a coating-bar with a 0.1 mm interval and 9 μm-depth grooves (OSG system products OSP-03) was set onto the substrate. The sample solution of 10 g L^{−1} with chlorobenzene, which was prepared by ultrasonic stirring and filtered through a PTFE membrane, was dropped onto the coating-bar, and then the coating-bar was moved in the horizontal direction at a speed of 33 μm s^{−1} by a brushless motor (Oriental Motor, BXS230A-10S). Thus 150 nm-thick uniform films were successfully obtained. The film fabrication was carried out in atmospheric air. Subsequently, a 3 nm-thick MoO₃ layer and a 150 nm-thick Ag electrode were deposited onto the bar-coated film of the mixture of **4** and **5** at approximately 1.0 nm s^{−1} under 10^{−5} Pa in a vacuum evaporator (Eiko Engineering, EO-5) to complete the device structure of ITO/**4** + **5** mixture/MoO₃/Ag. The active area of the sandwich device was 2 × 2 mm².

6.4 J–V measurements

Current density–voltage (*J–V*) characteristics of the device were measured using a source meter (KEITHLEY, 2400) without/with illumination of 100 mW cm^{−2} from a solar simulator equipped with an AM1.5G filter (Bunkoukeiki, OTENTO-SUN III).

Author contributions

The manuscript was written by MD and ML through contributions from all authors. MD synthesized all the materials and studied the LC and optical properties. Models were generated by MD and ML. GU, AF and MO recorded the film data. All authors have given approval to the final version of the manuscript.

Abbreviations

CPI	Complementary polytopic interaction
DCM	Dichloromethane
DIC	Diisopropylcarbodiimide
DMAE	Dimethylaminoethanol
DPTS	Dimethylaminopyridinium toluene sulfonate
NBS	<i>N</i> -Bromosuccinimide
Pd(dppf)Cl ₂	(1,1-Bis(diphenylphosphino)-ferrocene)palladium(II) dichloride
PPTS	Pyridinium toluene sulfonate
<i>p</i> TsOH	<i>p</i> -Toluenesulfonic acid
THF	Tetrahydrofuran

Conflicts of interest

There are no conflicts to declare.

Acknowledgements

We are grateful to the Deutsche Forschungsgemeinschaft (DFG) for their financial support within the LE1571/8-1.

Notes and references

- J. Ksters, P. Verstappen, M. Kelchtermans, L. Lutsen, D. Vanderzande and W. Maes, *Adv. Energy Mater.*, 2015, **5**, 1500218.
- G. de la Torre, G. Bottari and T. Torres, *Adv. Energy Mater.*, 2017, **7**, 1601700.
- H. Imahori, T. Umeyama, K. Kurotobi and Y. Takano, *Chem. Commun.*, 2012, **48**, 4032–4045.
- C.-L. Wang, W.-B. Zhang, H.-J. Sun, R. M. Van Horn, R. R. Kulkarni, C.-C. Tsai, C.-S. Hsu, B. Lotz, X. Gong and S. Z. D. Cheng, *Adv. Energy Mater.*, 2012, **2**, 1375–1382.
- C.-L. Wang, W.-B. Zhang, R. M. Van Horn, Y. Tu, X. Gong, S. Z. D. Cheng, Y. Sun, M. Tong, J. Seo, B. B. Y. Hsu and A. J. Heeger, *Adv. Mater.*, 2011, **23**, 2951–2956.
- M. Loi, P. Denk, H. Hoppe, H. Neugebauer, D. Meissner, C. Winder, C. Brabec, N. S. Sariciftci, A. Gouloumis, P. Vázquez and T. Torres, *Synth. Met.*, 2003, **137**, 1491–1492.
- J. Ranta, M. Niskanen, K. Kaunisto, V. Manninen, M. E. Mundy, K. Virkki, H. Hakola, T. I. Hukka and H. Lemmetyinen, *J. Porphyrins Phthalocyanines*, 2014, **18**, 1108–1124.
- A. Tolkkki, K. Kaunisto, A. Efimov, H. Kivistö, L. Storbacka, R. Savikoski, K. Huttunen, S. Lehtimäki and H. Lemmetyinen, *Phys. Chem. Chem. Phys.*, 2012, **14**, 3498–3504.
- A. Alekseev, N. Tkachenko, A. Efimov and H. Lemmetyinen, *Russ. J. Phys. Chem. A*, 2010, **84**, 1230–1241.
- N. V. Tkachenko, V. Chukharev, P. Kaplas, A. Tolkkki, A. Efimov, K. Haring, J. Viheriälä, T. Niemi and H. Lemmetyinen, *Appl. Surf. Sci.*, 2010, **256**, 3900–3905.
- K. Kaunisto, H. Vahasalo, V. Chukharev, N. V. Tkachenko, P. Vivo, M. Niemi, A. Tolkkki, A. Efimov and H. Lemmetyinen, *Thin Solid Films*, 2009, **517**, 2988–2993.
- H. Neugebauer, M. A. Loi, C. Winder, N. S. Sariciftci, G. Cerullo, A. Gouloumis, P. Vázquez and T. Torres, *Sol. Energy Mater. Sol. Cells*, 2004, **83**, 201–209.
- A. de la Escosura, M. V. Martínez-Díaz, J. Barberá and T. Torres, *J. Org. Chem.*, 2008, **73**, 1475–1480.
- Y. H. Geerts, O. Debever, C. Amato and S. Sergeev, *Beilstein J. Org. Chem.*, 2009, **5**, 49.
- M. Ince, M. V. Martínez-Díaz, J. Barberá and T. Torres, *J. Mater. Chem.*, 2011, **21**, 1531–1536.
- H. Hayashi, W. Nishashi, T. Umeyama, Y. Matano, S. Seki, Y. Shimizu and H. Imahori, *J. Am. Chem. Soc.*, 2011, **133**, 10736–10739.
- T. Kamei, T. Kato, E. Itoh and K. Ohta, *J. Porphyrins Phthalocyanines*, 2012, **16**, 1261–1275.
- M. Shimizu, L. Tauchi, T. Nakagaki, A. Ishikawa, E. Itoh and K. Ohta, *J. Porphyrins Phthalocyanines*, 2013, **17**, 264–282.
- L. Tauchi, T. Nakagaki, M. Shimizu, E. Itoh, M. Yasutake and K. Ohta, *J. Porphyrins Phthalocyanines*, 2013, **17**, 1080–1093.
- A. Ishikawa, K. Ono, K. Ohta, M. Yasutake, M. Ichikawa and E. Itoh, *J. Porphyrins Phthalocyanines*, 2014, **18**, 366–379.
- M. Yoshioka, K. Ohta, Y. Miwa, S. Kutsumizu and M. Yasutake, *J. Porphyrins Phthalocyanines*, 2014, **18**, 856–868.
- A. Watarai, S. n. Yajima, A. Ishikawa, K. Ono, M. Yasutake and K. Ohta, *ECS Trans.*, 2015, **66**, 21–43.
- A. Watarai, K. Ohta and M. Yasutake, *J. Porphyrins Phthalocyanines*, 2016, **20**, 1444–1456.
- M. Lehmann, M. Dechant, M. Holzapfel, A. Schmiedel and C. Lambert, *Angew. Chem., Int. Ed.*, 2019, **58**, 3610–3615.
- M. Lehmann, M. Dechant, M. Lambov and T. Ghosh, *Acc. Chem. Res.*, 2019, **52**, 1653–1664.
- M. Lehmann, M. Dechant, L. Gerbig and M. Baumann, *Liq. Cryst.*, 2019, **46**, 1985–1994.
- T. Brunet, O. Thiebaut, E. Charlet, H. Bock, J. Kelber and E. Grelet, *EPL*, 2011, **93**, 16004.
- H. Meier, *Angew. Chem., Int. Ed. Engl.*, 1992, **31**, 1399–1420.
- M. Scheuble, M. Goll and S. Ludwigs, *Macromol. Rapid Commun.*, 2015, **36**, 115–137.
- E. O. Arikainen, N. Boden, R. J. Bushby, O. R. Lozman, J. G. Vinter and A. Wood, *Angew. Chem., Int. Ed.*, 2000, **39**, 2333–2336.
- M. Bai, R. Song, Y. Zhang, S. Han, X. Song and F. Meng, *Inorg. Chem. Commun.*, 2013, **28**, 99–103.
- A. D. Garland, I. Chambrier, A. N. Cammidge and M. J. Cook, *Tetrahedron*, 2015, **71**, 7310–7314.
- M. Lehmann and M. Hügél, *Angew. Chem., Int. Ed.*, 2015, **54**, 4110–4114.

- 34 M. Hügel, M. Dechant, N. Scheuring, T. Ghosh and M. Lehmann, *Chem. – Eur. J.*, 2019, **25**, 3352–3361.
- 35 M. T. Zhao, B. P. Singh and P. N. Prasad, *J. Chem. Phys.*, 1988, **89**, 5535–5541.
- 36 H. Meier, U. Stalmach and H. Kolshorn, *Acta Polym.*, 1997, **48**, 379–384.
- 37 A. T. Bilgiçli, A. Günsel, M. Kandaz and A. R. Özkaya, *Dalton Trans.*, 2012, **41**, 7047–7056.
- 38 M. Kasha, *Radiat. Res.*, 1963, **20**, 55–70.
- 39 M. Kasha, *Discuss. Faraday Soc.*, 1950, **9**, 14–19.
- 40 A. de la Escosura, M. V. Martínez-Díaz, D. M. Guldi and T. Torres, *J. Am. Chem. Soc.*, 2006, **128**, 4112–4118.
- 41 M. Krug, C. Stangel, A. Zieleniewska, T. Clark, T. Torres, A. G. Coutsolelos and D. M. Guldi, *ChemPhysChem*, 2019, **20**, 2806–2815.
- 42 M. A. Loi, P. Denk, H. Hoppe, H. Neugebauer, D. Meissner, C. Winder, C. J. Brabec, N. S. Sariciftci, A. Gouloumis, P. Vázquez and T. Torres, *Synth. Met.*, 2003, **137**, 1491–1492.
- 43 M. Ahmida, R. Larocque, M. S. Ahmed, A. Vacaru, B. Donnio, D. Guillon and S. H. Eichhorn, *J. Mater. Chem.*, 2010, **20**, 1292–1303.
- 44 P. Apostol, J. Eccher, M. E. R. Dotto, C. B. Costa, T. Cazati, E. A. Hillard, H. Bock and I. H. Bechtold, *Phys. Chem. Chem. Phys.*, 2015, **17**, 32390–32397.
- 45 N. Zharnikova, N. Usol'tseva, E. Kudrik and M. Thelakkat, *J. Mater. Chem.*, 2009, **19**, 3161–3167.
- 46 J. Rittich, S. Jung, J. Siekmann and M. Wuttig, *Phys. Status Solidi B*, 2018, **255**, 1800075.
- 47 Y. Wang, J. Chen, H. D. Kim, B. Wang, R. Iriguchi and H. Ohkita, *Front. Energy Res.*, 2018, **6**, 113.
- 48 J. Eccher, G. C. Faria, H. Bock, H. von Seggern and I. H. Bechtold, *ACS Appl. Mater. Interfaces*, 2013, **5**, 11935–11943.
- 49 J. Eccher, W. Zajaczkowski, G. R. C. Faria, H. Bock, H. Von Seggern, W. Pisula and I. H. Bechtold, *ACS Appl. Mater. Interfaces*, 2015, **7**, 16374–16381.
- 50 G. Uzurano, Y. Yabuuchi, R. Ishiura, M. Yoneya, S. Nagano, A. Fujii and M. Ozaki, *Jpn. J. Appl. Phys.*, 2019, **59**, SDDA05.
- 51 P. A. Heiney, 2006, <http://www.datasqueezesoftware.com>.
- 52 P. Scherrer, *Nachr. Ges. Wiss. Goettingen, Math.-Phys. Kl.*, 1918, **2**, 98–100.